Molecular Dynamics Simulations of Valinomycin and Its Potassium Complex in Homogeneous Solvents

T. R. Forester,* W. Smith,* and J. H. R. Clarke#
*CCLRC Daresbury Laboratory, Daresbury, Cheshire WA4 4AD, UK, and #Department of Chemistry, UMIST, Manchester M60 1QD, UK

ABSTRACT Molecular dynamics simulations of kalinomycin (VM) and its potassium complex in water and in a Lennard Jones solvent are reported. In agreement with experimental evidence the structure of K^+-VM in nonpolar solution is similar to the solid state structure whereas the structure of uncomplexed VM is not. In water uncomplexed VM retains the Lac and HyV faces (which are lost in nonpolar solution) and shows some similarity with the solid-state structure obtained by crystallization from dimethyl sulfoxide (DMSO). However, also in agreement with spectroscopic data a dynamic equilibrium between a set of conformers is established in both solvents. Our model reproduces the experimental dipole moment (3.6 D) of VM in nonpolar solution. We also observed the spontaneous decomplexation of K^+-VM in water, with the ion passing through the HyV face in preference to the Lac face. Water attack was observed through both faces. The time scale for all conformational transitions is of the order of 100 ps, with structural changes associated with the (de)-complexation reaction controlled by the ring dihedrals in the vicinity of the L-lactic acid residues. Global structural functions, radial distribution functions, and VM ring dihedral analysis are presented, along with an analysis of the decomplexation event.

INTRODUCTION

Valinomycin (VM) is a naturally occurring antibiotic ionophore that actively transports potassium through the cell walls of living tissue. As a cyclodepsipeptide (Fig. 1) it is a relatively simple biological molecule, but with considerable conformational flexibility. In complexes of VM with alkali metal ions in the solid state, the VM folds around the ion with the ring adopting a "tennis ball seam" arrangement. NMR, infrared (IR), and Circular Dichroism (CD) measurements indicate that the conformational structure of the K^+-VM complex in chloroform, methanol, and cell vesicles is similar to the solid state, though the complex itself is unstable in water (Grell and Funck, 1975).

The uncomplexed molecule can be crystallized into a number of conformers including the "twisted bracelet" (TB) conformation from octane (Karle, 1975) and the "twisted propeller" (TP) conformation from DMSO (Karle and Flippen-Anderson, 1988). In solution the structural data are much less clear, but conformations adopted by VM seem to reflect the polarity of the solvent (Bystrov et al., 1977): one set of conformers predominates in nonpolar solvent, whereas another predominates in more polar environments, such as methanol-water mixtures. Regardless of the solvent, however, no single conformational state predominates at room temperature nor are spectroscopic measurements Ultra-Violet (UV), CD, IR, and NMR) of VM fully consistent with the existence in solution of any of the solid-state conformers (Grell and Funck, 1975; Feigenson and Meers, 1980; Jackson and Mantsch, 1991).

Clearly, an understanding of the solvent-induced conformations of VM (and K^+-VM) is of central importance in explaining its ability to facilitate ion transport across the water-membrane interface. Ideally it would be useful to have clear-cut structural data on VM adsorbed at such an interface but no experimental data are available. One of the aims of this article is to show that structural data from computer simulations can be used to build an understanding of structural effects in VM and then to enhance the interpretation of experimental data. Preliminary to explicit simulation of antibiotic action at the interface, we report a molecular dynamics (MD) study of VM and the K^+-VM complex in nonpolar and aqueous solution. These solvents mimic the environments expected on either side of the cell interface viz the interior of the lipid bilayer of the cell wall and the water on either side of the cell wall.

In the next section, we give a description of the computational details and outline the approach we have used to characterize structure and structural changes in this complex system. In Results and Discussion we present and discuss the results obtained for the structure of VM and the K^+-VM complex in the Lennard-Jones solvent and in water; the complex is unstable in water and we give details of the mechanism of the decomplexation.

COMPUTATIONAL METHODOLOGY

Molecular dynamics simulations

The MD methods adopted in this study are closely related to those in our previous work on the VM and K^+-VM systems (Forester et al., 1994; Forester et al., 1995). Four simulations were undertaken, each at a temperature of 310 K and 300 ps in length, including a period of 50 ps for initial equilibration of the system. The simulations were performed using a 16-processor IBM SP2 parallel computer at Daresbury Laboratory, and the 256 processor Cray-T3D at the Edinburgh Parallel Computing Centre. The simulated systems were 1) VM in a Lennard-Jones (LJ) solvent; 2) VM in water; 3) K^+-VM in LJ solvent; and 4) K^+-VM in water.

Received for publication 20 February 1996 and in final form 14 May 1996.
Address reprint requests to Dr. T. R. Forester, CC RC Daresbury Laboratory, Keckwick Lane, Daresbury, Cheshire WA4 4AD, UK. Tel.: 44-1925-603257; Fax: 44-1925-603634; E-mail: trf@dl.ac.uk.

0006-3495/96/08/544/10 $2.00

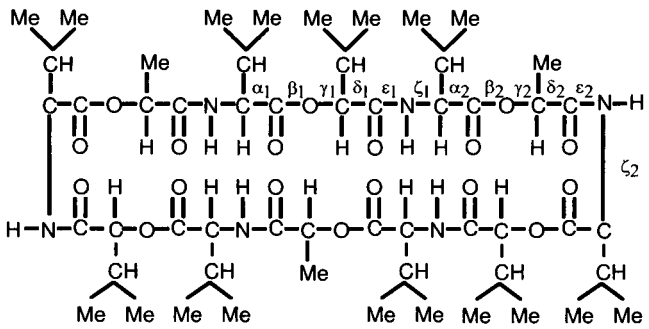

FIGURE 1 Chemical structure of Valinomycin (VM). Ring dihedral angles ($\alpha_1 - \zeta_2$) are identified by the central atom pair. The molecule is made from three (L-Val-D-HyV-D-Val-L-Lac) units.

The chosen model for water was the simple point charge (SPC) potential (Berendsen et al., 1981). Lennard Jones solvent has recently been successfully used to represent a biological membrane (Guba and Kessler, 1994; Roux et al., 1995). In our previous work an adapted AMBER force field (Weiner et al., 1986) was employed to model both K^+-VM and VM in the solid state and in vacuo (Forester et al., 1994); in addition it was used to model the spontaneous capture of partially solvated K^+ (Forester et al., 1995). The same adapted AMBER force field was used here also. The usual Berthelot combining rules were used for solute-solvent interactions. The forcefield we used does have some limitations, notably that there is no adjustment made for ion-induced polarization on the solvent or the biopolymer. Consequently the strength of K^+ binding to VM (and to the solvent) will be underestimated. Moreover, as Marrone and Merz (1995), who also used an AMBER-based force field, noted there are difficulties in finding a static set of partial charges that faithfully model the electrostatics of uncomplexed VM in its different conformational states. Our force field undoubtedly suffers from the same limitations, although as mentioned above it has proved robust in simulations of complexed and uncomplexed VM in a number of environments.

All the simulations reported here utilized a truncated octahedral (TO) MD cell based on a cube of length ~45 Å. TO boundary conditions are considerably more efficient than a standard cubic cell as they reduce the number of solvent molecules in the system for a given maximum potential cutoff. Periodic boundary conditions were implemented to prevent surface effects perturbing the calculations.

In the two LJ solvent simulations a standard Coulombic potential was used with a cutoff of 20 Å. This was sufficient to ensure all VM sites interacted with each other but not with sites of solute molecules in neighboring cells. The calculations thus effectively modeled VM or K^+-VM at infinite dilution. The simulation cell contained 500 solvent particles, which had LJ interaction parameters of $\epsilon = 598.6$ J mol^{-1}, $\sigma = 3.923$ Å, the same as used for methylene groups in hydrocarbon membranes (Bishop and Clarke, 1991).

For the two simulations in water, an Ewald sum (Smith and Fincham, 1993) with energies and forces converged to one part in 10^{-6} was used to calculate the electrostatic terms. The cell contained 1223 water molecules in addition to the solute; the effective concentration of VM was 30 mmol/dm^{-3}. The use of the Ewald sum was necessary to avoid structural and dynamical artifacts arising from the truncation of electrostatic interactions (Schreiber and Steinhauser, 1992; Lau et al., 1994; Perera et al., 1995).

All simulations were performed using the parallel molecular dynamics package DL_POLY (Smith and Forester, 1994a; Smith and Forester, 1994b; Forester and Smith, 1994). The equations of motion were solved using the Verlet leapfrog algorithm with a time step of 2 fs. A controlled pressure algorithm (Melchionna et al., 1993) was used to allow the cell volume to adjust during the equilibration portion of the simulations and to obtain a mean pressure close to atmospheric. The production portion of the simulations were carried out in the canonical ensemble (constant NVT) with temperature coupled to a Nosé-Hoover thermostat (Hoover, 1985). All bond lengths were constrained by application of the parallel SHAKE algorithm, RD-SHAKE (Smith and Forester, 1994b). In all four simulations the nonelectrostatic pair interactions (e.g., Lennard-Jones and hydrogen-bonding potentials) were truncated at 12 Å.

Structure characterization

As in previous studies (Forester et al., 1994; Forester et al., 1995) we have measured some aspects of the global structure of VM. The first was the asphericity order parameter, A_3 (Rudnick and Gaspari, 1987)

$$A_3 = \frac{\langle \sum_{i \neq j} (\lambda_i - \lambda_j)^2 \rangle}{2\langle (\sum_{i=1}^{3} \lambda_i)^2 \rangle} \tag{1}$$

where $\langle \ldots \rangle$ denotes an ensemble average and the λ_i are the three principal moments of inertia of the molecule. A_3 is 0 for a perfectly spherical object, 0.167 for an infinitely thin disk, and 1.0 for an infinitely thin rod.

The second measure of global structure calculated was the mean-squared radius of gyration, S^2, defined as

$$S^2 = \frac{1}{M} \sum_{i=1}^{N} m_i \| r_i - r_{com} \|^2 \tag{2}$$

where M is molecular mass, r_i the position of the ith atom, m_i its mass, and r_{com} the position of the VM center of mass.

The conformational state of the VM or K^+-VM can be defined in terms of the 36 ring dihedral angles, which are grouped in 12 distinct types. These are indicated in Fig. 1. Each of the angles may be classified as gauche ($g+$ or $g-$) or trans (t), the complete specification of which uniquely defines the structure. All three sets of angles for the TB and TP conformers and for the K^+-VM forms are shown in columns 2, 3, and 6, respectively, of Table 1. In all three cases the atomic coordinates were taken from crystallographic data. In each structure the VM has two distinct faces, and in the case of K^+-VM it is through these faces that potassium (de-)complexation is thought to take place. The faces are evident in the molecular structures (Fig. 2 *a–c*). The Lac face contains the three methyl groups from the L-lactic acid residues and three isopropyl groups from the D-Valine residues, and involves the angles $\alpha_2 - \zeta_2$. The HyV face is more bulky; it contains six isopropyl groups from the three HyV residues and the three L-Valine residues, and its conformation is defined by the angles $\alpha_1 - \zeta_1$. A number of general features are evident from the data in Table 1, such as rigidity of the β and ϵ dihedrals and the almost perfect regularity of the K^+-VM structure. However, it is noticeable that neither the TB nor the TP structure has perfect threefold symmetry (which requires that all three angles of a given type have the same conformation). The presence of the Lac and HyV faces appears to be relatively insensitive to at least some of the dihedral types (e.g., γ_2 and δ_2) that are key to some of the structural transitions we observe. The key parameters that we use in discussing the conformational changes underlying the decomplexation reaction are δ_2 and, to a lesser extent, the α_2 and γ_2 dihedral angles, which are all in the neighborhood of the L-lactic acid residues.

We shall also discuss local solvation effects in terms of partial radial distribution functions (RDFs), from which the extent of solvation around each site can be obtained by integrating the partial RDFs. The integral coordination number, $n_{\alpha\beta}(r)$, which gives the mean number of β sites within a sphere of radius r around an α site, is defined as

$$n_{\alpha\beta}(r) = 4\pi\rho_\beta \int_0^r x^2 g_{\alpha\beta}(x)\, dx. \tag{3}$$

Where $g_{\alpha\beta}(r)$ is the partial RDF between atoms of types α and β, and ρ_β is the number density of β sites in the system. Throughout this article we use the following notation to denote VM and water sites: "CT" is the sp^3 hybridized carbon; "C" the sp^2 carbon; "H" the amide hydrogen; "N" the

TABLE 1 Dihedral conformations of representative VM configurations

Dihedral	VM(TB)*			VM(TP)#			VM(LJ)			VM(H_2O)			K^+-VM§			K^+-VM(H_2O)$_1$			K^+-VM(H_2O)$_2$		
α_1	t	t	$g-$	t	$g-$	$g-$	$g-$	t	$g-$	t	$g-$	$g-$	t	t	t	t	t	$g-$	t	$g-$	$g-$
β_1	t	t	t	t	t	t	t	t	t	t	t	t	t	t	t	t	t	t	t	t	t
γ_1	$g-$	$g-$	t	$g-$	$g-$	$g-$	$g-$	$g-$	$g-$	$g-$	$g-$	$g-$	$g-$	$g-$	$g-$	$g-$	$g-$	$g-$	$g-$	$g-$	$g-$
δ_1	$g-$	$g+$	$g+$	$g+$¶	$g-$	$g-$	$g-$	$g-$	$g-$	$g-$	$g-$	$g-$	$g-$	$g+$¶	$g-$	$g-$	$g-$	$g-$	$g-$	$g-$	$g-$
ϵ_1	t	t	t	t	t	t	t	t	t	t	t	t	t	t	t	t	t	t	t	t	t
ζ_1	$g-$	$g-$	$g-$	$g-$	$g-$	$g-$	$g-$	$g-$	$g-$	$g-$	$g-$	$g-$	$g-$	$g-$	$g-$	$g-$	$g-$	$g-$	$g-$	$g-$	$g-$
α_2	t	$g+$	t	t	t	t	$g+$	t	$g-$	$g+$	$g+$	$g+$	t	t	t	$g+$	t	$g+$	t	t	t
β_2	t	t	t	t	t	t	t	t	t	t	t	t	t	t	t	t	t	t	t	t	t
γ_2	$g+$	t	$g+$	t	t	t	t	t	t	t	t	t	$g+$	$g+$	$g+$	$g+$	$g+$	$g+$	$g+$	$g+$	$g+$
δ_2	$g-$	$g-$	$g+$	$g-$	$g-$	$g-$	$g-$	$g-$	$g+$	$g-$	$g-$	$g+$	$g+$	$g+$	$g+$	$g+$	$g+$	$g+$	$g-$	$g-$	$g-$
ϵ_2	t	t	t	t	t	t	t	t	t	t	t	t	t	t	t	t	t	t	t	t	t
ζ_2	$g+$	$g+$	$g+$	$g+$	$g+$	$g+$	t	$g+$	$g+$	$g+$	t	$g+$	$g+$	$g+$	$g+$	$g+$	$g+$	$g+$	$g+$	t	$g+$

*Crystal structure from Karle (1975).
#Crystal structure from Karle and Flippen-Anderson (1988).
§Crystal structure from Neupert-Laves and Dobler (1975).
¶Close to the g^-/g^+ borderline.

amide nitrogen; "O" the oxygen of the amide carbonyl; "Oe" the oxygen of the ester carbonyl; "Os" the ester linkage oxygen; "Ow" the water oxygen; and "Hw" the water hydrogen.

RESULTS AND DISCUSSION

Uncomplexed VM in the apolar LJ solvent

The starting structure for this simulation was a VM molecule taken from the TB crystal structure and surrounded by 500 LJ particles. Some of the global properties of VM in the LJ solvent are shown in Table 2, and a snapshot of the structure is shown in Fig. 2 *d*. There are some similarities, e.g., in the values of A_3 and S^2, with the crystalline TB and TP structures, but there are, however, several mismatches (S^2 with the TP structure, the dipole moment μ with the TB structure) that, suggest, in agreement with the conclusions of experimental studies, that the structure in solution is not the same as in the associated crystal. The high conformational flexibility of VM has already been referred to and it is quite possible that under the influence of solvent interactions there is a range of closely related conformations in dynamic equilibrium. In the case of the TB structure obtained from *n*-octane, there is considerable symmetry in the distribution of polar carbonyl groups and the associated H-bonds, so it is perhaps not surprising that this conformer has a low dipole moment (the value quoted in Table 2 was calculated using experimental structural data and using our charge distribution). The much larger value observed in solution, which agrees closely with the experimental value measured in CCl_4 (Ivanov et al., 1969), suggests a greater degree of structural disorder.

The conformational structure of VM in the LJ solvent is included in Table 1; once again we see some similarities in the pattern of dihedral angles with either (for γ_1 or δ_2) or both (β and ϵ) the TB and TP crystalline forms. However, we can extend the picture further by examining the data in Table 3, which gives the percentage of each conformation adopted by a particular dihedral type in the course of the simulation. Because there are three sets of each of the 12 dihedral types, if one conformer predominated in a solvent each entry in Table 3 would be a multiple of 33.3%. Although this is found for some individual dihedrals (e.g., the β and ϵ and α_2 for VM in the LJ solvent), it is not so for all the dihedrals, e.g., α_1, ζ_1, and ζ_2. The values given in Table 3 (for all systems) were from averages taken over the 250-ps production period of the simulation. They were little different from the averages obtained over the first 150 ps of the same period. Larger fluctuations were seen if a 50-ps window was used for the averages. These results imply that there is a dynamic equilibrium between a number of conformers in solution with a time scale for conformational relaxation of about 100 ps. This is ~10 times faster than the experimental estimates of VM conformational relaxation times (Grell and Funck, 1975) but shows agreement with the experiment in that an equilibrium is established between different sets of conformers in solution.

The RDFs for solvent molecules around some of the VM sites are shown in Fig. 3 *a*, whereas estimates for the $n(r)$ are collated in Table 4. In this solvent $n(r)$ was evaluated out to $r = 1.5 \times 2^{1/6}\sigma_{\alpha LJ}$, the position of the first minimum in $g_{\alpha LJ}(r)$ in a liquid mixture of nonbonded, neutral, α, and LJ particles. The applied cutoffs were thus 4.80 Å (α = H), 5.36 Å (HC), 5.70 Å (O, Oe, Os), 5.93 Å (N), 6.00 Å (CT), and 6.08 Å (C).

Fig. 3 *a* and Table 4 also include the solvent-solvent functions for reference. The solvent was found to have all the characteristics of a well-behaved LJ liquid; the coordination number was close to 12 (Table 4) and $g_{LJLJ}(r)$ had clear first and second maxima. As would be expected from the hydrophobic nature of the solvent, the alkyl groups were the most strongly solvated of the VM sites. Also of note is that the ester carbonyls (Oe) were considerably less solvated than the amide carbonyls (O), a feature that was reproduced in all four simulations. The ester linkage oxygen (Os) did

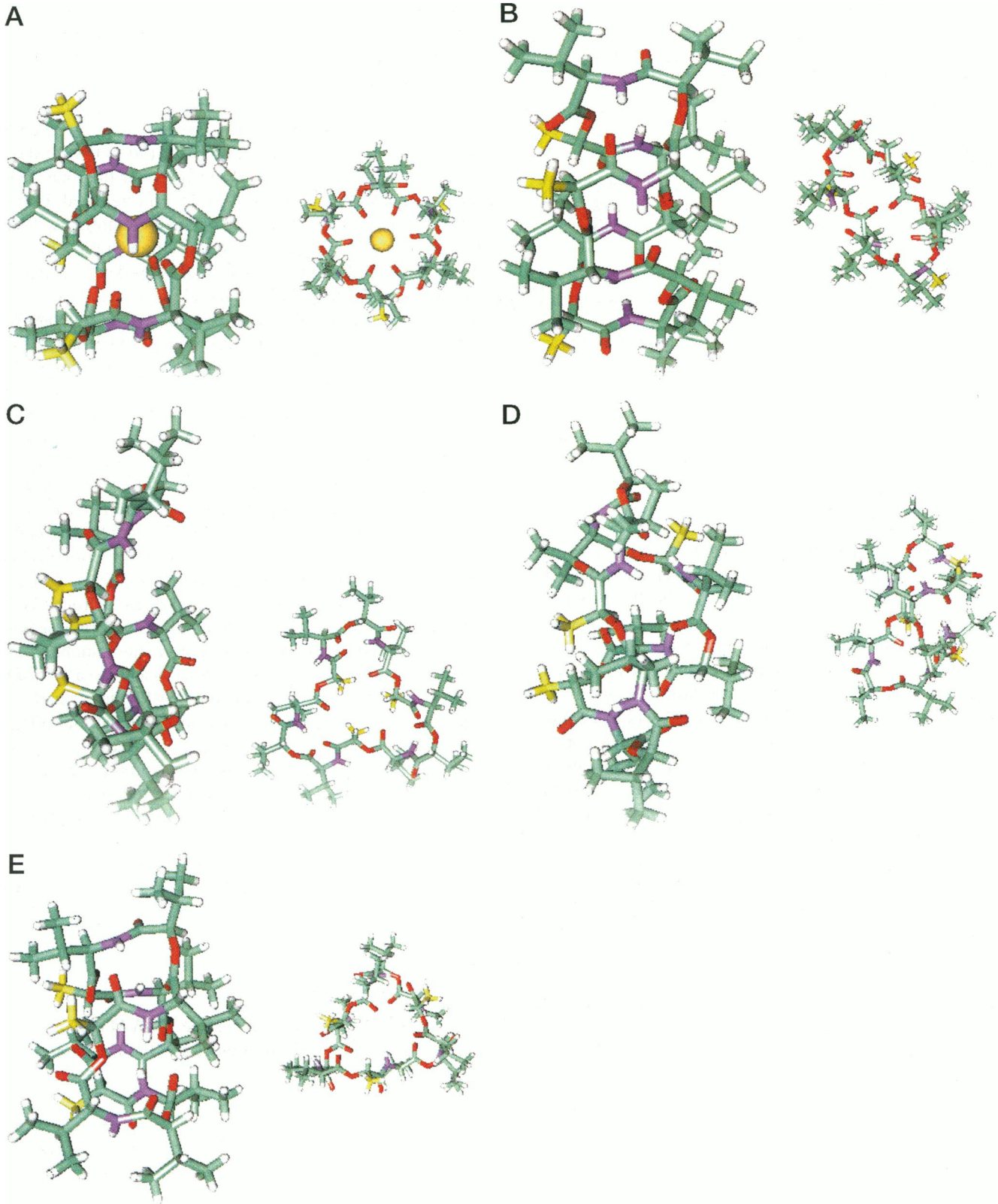

FIGURE 2 Snapshots of representative valinomycin (VM) structures. In each case the color scheme is as follows: methyl carbon of the lac residues (*yellow*), all other carbons (*green*), oxygen (*red*), nitrogen (*purple*), hydrogen (*grey*). In each case a view is shown along two orthogonal directions. In the first view the Lac face is on the left and the HyV face on the right. In the second view the Lac face is at the back and the HyV at the front of the structure. (*a*) The K^+-VM crystal structure (Neupert-Laves and Dobler, 1975). The potassium is drawn as a sphere in the center of the structure. (*b*) The twisted bracelet (TB) crystal structure (Karle, 1975). (*c*) The twisted propellar (TP) crystal structure (Karle and Flippen-Anderson, 1988). (*d*) VM in a Lennard-Jones solvent. The Lac and HyV faces are no longer present. (*e*) VM in water.

TABLE 2 Conformational properties of VM and K^+-VM at 310 K

	A_3	S^2/Å^2	μ/D
VM Environment			
TB (Karle, 1975)*	0.160	28.5	1.39
TP (Karle and Flippen-Anderson, 1988)*	0.164	38.2	3.54
CCl_4 (expt) (Ivanov et al., 1969)	—	—	3.5
in vacuo (Forester, et al., 1994)	0.15	29.5	3.6
LJ	0.16	29.8	3.7
water	0.07	30.3	2.7
K^+-VM Environment			
Crystal (Neupert-Laves and Dobler, 1975)	0.04	27.5	1.41
in vacuo (Forester et al., 1994)	0.02	27.5	3.2
LJ	0.07	28.5	3.1

*μ calculated with our charge set.
Expt. values not available.

not show a clear first solvation peak (Fig. 3 *a*) and was effectively hidden from close contact with solvent.

Uncomplexed VM in water

The starting structure for this simulation was a VM molecule taken from the TB crystal structure and surrounded by 1223 SPC water molecules. VM is practically insoluble in water so there is no experimental data with which we can make close comparisons. However, the structural data from the simulations, which is summarized in Tables 1–4, can be compared with those of the TP conformer, which is crystallized from the moderately polar DMSO. There are indeed some similarities. Viewed down the axis of the pore, the molecule has almost trigonal symmetry in both cases (Fig. 2 *c* and *e*), and dihedral conformations (Table 1) differed only in that for the aqueous structure α_2 was predominantly $g+$, whereas in the TP crystal they were t. In addition, in water VM has on average one ζ_2 t for half the time, whereas in the TP crystal they are always $g+$. Nonetheless, the TP conformer was considerably more disklike than VM in water and, therefore, had a much larger mean-squared radius of gyration (Table 2).

A selection of the water RDFs are shown in Fig. 4, and the integral coordination numbers are given in Table 4. The Ow coordination numbers were calculated in a similar manner to those in LJ solvent. In this case, the cutoff criterion was determined from the clear minimum in $g_{OOw}(r)$, and cutoffs for other sites were obtained by adding the difference between the Lennard-Jones σ for the site and the value of σ_O. The cutoff radii used were: 2.77 Å (H), 3.32 Å (HC), 3.41 Å (O, Oe, Os), 3.53 Å (N), 3.57 Å (CT), and 3.62 Å (C). Two points are noteworthy. First, comparing the coordination numbers in Table 4 for water [n(Ow)] with those for LJ solvent [n(LJ)], it was apparent that the total coordination numbers around the VM sites are reduced. In part this is because of the significantly smaller cutoffs used, but it is also a consequence of the quasi-tetrahedral packing of water (4–5 neighbors) versus the closest packed structure of LJ solvent (≈12 neighbors). Second, the order of solvation in water is significantly changed from that in nonpolar solvent. In water it is the polar carbonyl oxygens (O, Oe) that are the most heavily solvated, whereas solvation of the CT sites is reduced from the high value in LJ solvent to be on a par with that of the amide nitrogen. The solvation of the carbonyl oxygens in water is primarily due to hydrogen bonding. This can be seen from an analysis of the RDFs in Fig. 4 *b* and the coordination numbers (n(Hw) and n(Ow)) in Table 4. Values for n(Hw) were calculated at 0.81 Å less than the corresponding Ow function. As the Ow-Hw bond-length in the SPC model is 1 Å, this cutoff criterion gives a crude measure of the number of (near) linear hydrogen bonds to a given site. Indeed, if a site acts as hydrogen bond acceptor then one would expect to see a sharp first peak in $g_{\alpha Hw}(r)$ around 1.8 Å and a Hw coordination number close to the Ow coordination number. Such was the case for Oe and O sites but not for the remaining VM sites (which all, except for C, had values for n(Hw) less than half of n(Ow)). The first and second peaks in $g_{OeHw}(r)$ and $g_{OHw}(r)$ occurred at precisely the same positions as in the water-water function, $g_{OwHw}(r)$ (Fig. 4 *b*). As in LJ solvent, the amide carbonyls were more heavily solvated than the ester carbonyls and the Os sites were effectively hidden from the solvent. The amide hydrogen remained relatively unsolvated and showed only small amounts of hydrogen bonding to the solvent.

K^+-VM in LJ solvent

We have previously reported that the K^+-VM crystal structure can be reproduced using our force field. Although the

TABLE 3 Average dihedral conformations of VM and K^+-VM in solution

	%	α_1	β_1	γ_1	δ_1	ϵ_1	ζ_1	α_2	β_2	γ_2	δ_2	ϵ_2	ζ_2
VM (H_2O)	$g-$	38	—	97	95	—	96	—	—	—	92	—	—
	$g+$	—	—	—	5	—	—	73	—	28	3	—	83
	t	62	100	3	—	100	4	27	100	72	5	100	17
VM (LJ)	$g-$	55	—	100	98	—	76	33	—	—	63	—	—
	$g+$	—	—	—	2	—	—	33	—	2	37	—	77
	t	45	100	—	—	100	24	34	100	98	—	100	23
K^+-VM (LJ)	$g-$	34	—	100	96	—	99	—	—	—	1	—	31
	$g+$	23	—	—	4	—	—	22	—	100	99	—	64
	t	43	100	—	—	100	1	78	100	—	—	100	5

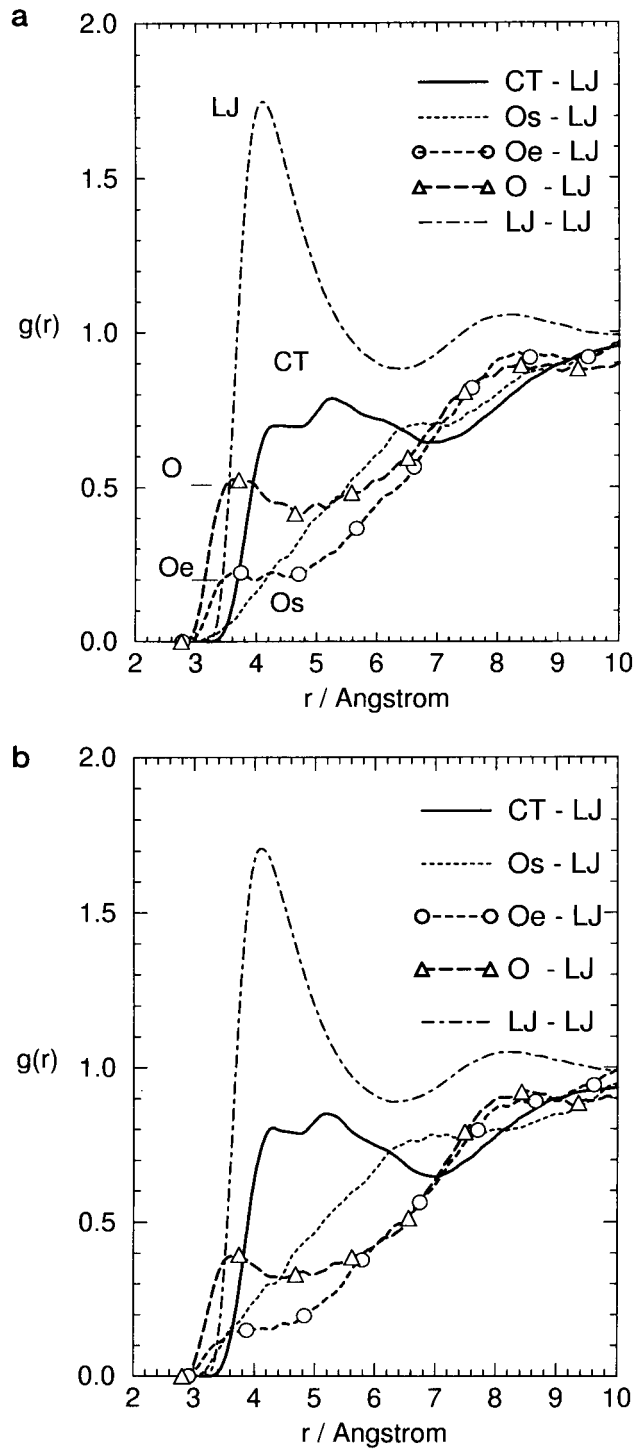

FIGURE 3 Valinomycin (VM)-LJ RDFs in (*a*) the VM (LJ) simulation and (*b*) the K^+-VM (LJ) system. CT are the alkyl carbons, Os the ester linkage oxygen, Oe the ester carbonyl oxygen, and O the amide carbonyl oxygen.

main features of the structure were retained in apolar solution, including clearly defined Lac and HyV faces, as in the simulations of K^+-VM in vacuo (Forester et al., 1994), some minor deviations from the crystal structure were apparent. Of particular interest was that an average of 2.0

TABLE 4 Integral coordination numbers of uncomplexed VM in solution

site	n(LJ)*	n(Ow)*	n(Hw)#
CT	4.95	0.48	0.04
O	2.98	1.34	1.10
C	2.92	0.27	0.21
N	2.23	0.43	0.08
Os	2.06	0.24	0.12
Oe	1.64	0.75	0.55
H	0.37	0.32	0.03
[LJ]	11.4	—	—
[Ow]	—	4.73	2.06
[Hw]	—	1.03	

*See text for values of cutoff radii used.
#RDFs integrated out to 0.81 Å less than the corresponding Ow RDF.

amide carbonyls entered the first coordination sphere of the cation and one ester carbonyl was displaced from it. (The first coordination sphere is defined to be 3.25 Å from the potassium.) This raised the K^+ coordination number to 7.0 from the solid-state value of 6.0. The coordination number for K^+ reported here is much the same as observed in in vacuo simulation of K^+-VM (Forester et al., 1994). This appears to introduce some lability in the complex because rapid exchange of amide carbonyls between first and second coordination spheres of the cation is apparent from the nonzero minimum in $g_{OK}(r)$ (Fig. 5). Fig. 5 also demonstrates that the Os oxygens remained only in the second coordination sphere of the cation. The RDFs with the solvent (Fig. 3 *b*) are broadly similar to those for uncomplexed VM (Fig. 3 *a*). However, in the case of the K^+-VM, the alkyl carbons are more exposed to the solvent and the carbonyl oxygens less exposed than in the uncomplexed form.

K^+-VM in water and the decomplexation reaction

A single complex from the K^+-VM crystal structure was used to prepare this solution. Because the experimental stability constant for K^+-VM in water is about 0.1 (Grell and Funck, 1975) decomplexation is expected to be spontaneous. Consequently during the equilibration period of 50 ps, harmonic restraints were applied to the six K-Oe distances to inhibit decomplexation. The force constant for each restraint was 70 kcal mol^{-1} $Å^{-2}$ and the equilibrium restraint length was 2.75 Å. Electrostatic and short-ranged interactions between the K^+ and Oe sites were evaluated in addition to the restraint terms. The restraints were removed at the start of the production portion of the simulation. We observed spontaneous decomplexation over a period of about 100 ps.

To examine the underlying structural changes free from uninteresting vibrational effects we have taken a series of configurations from points during this simulation and performed energy minimizations on the structures using a steepest descent method. Fig. 6 shows snapshots of two of the resultant conformers.

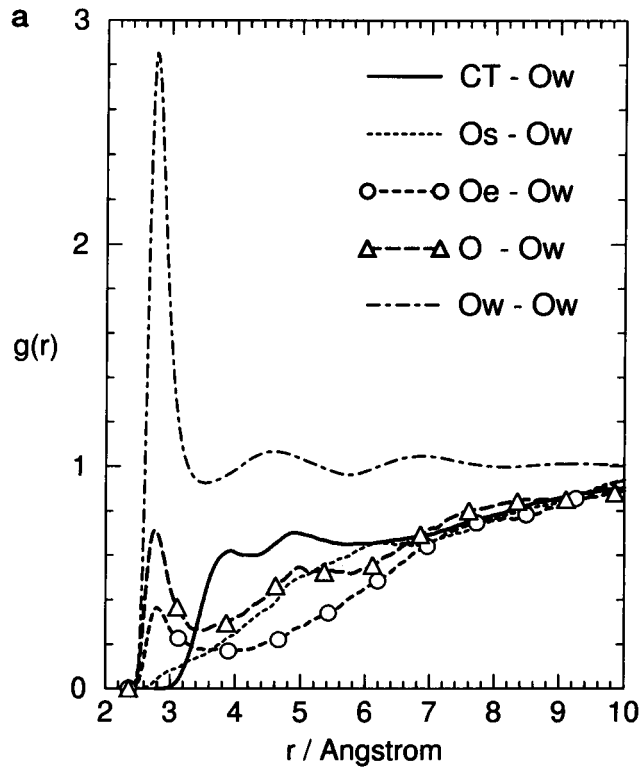

FIGURE 4 VM-water RDFs (*a*) for water oxygen (Ow) (*b*) for water hydrogen (Hw). VM site labels as in Fig. 3.

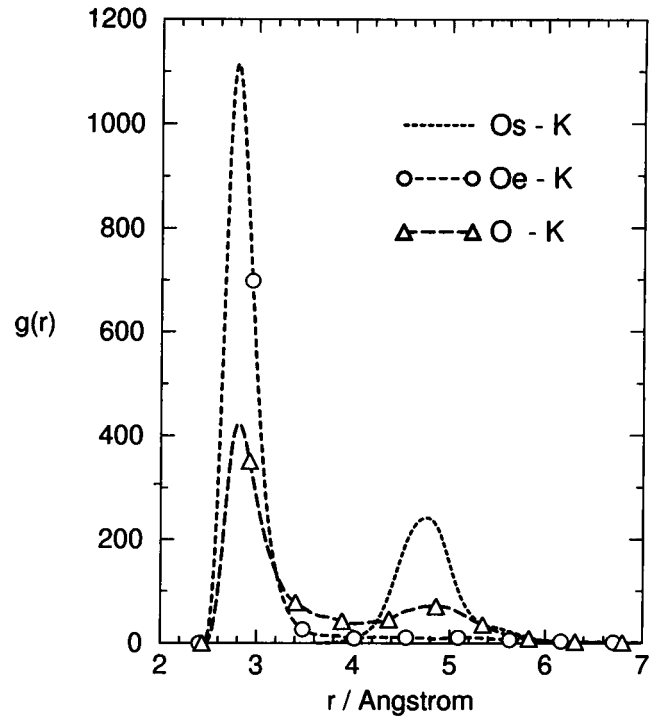

FIGURE 5 Oxygen-Potassium partial RDFs for the K^+-VM complex in LJ solvent. VM site labels as in Fig. 3.

The details of the decomplexation event may be monitored through the cation coordination number as a function of time (Fig. 7). In this figure we show coordination numbers of all potential oxygen ligands in the first and second hydration spheres of the cation. During the equilibration period (corresponding to $t < 0$), one water molecule approached the cation through the HyV face and another through the Lac face (Fig. 6 *a*). It is the former water that is the most closely coordinated. In this state there are five Oe ligands in the first shell (six if the shell is defined at 3.5 Å rather than 3.25 Å). On removal of the restraints another water is added through the HyV face (after 5 ps), which then displaces one of the Oe groups. However it is after ~25 ps that more major changes occur. In the first solvation shell the process is principally one of exchange of Oe ligands for water, although as the K^+ moves away from the center of the VM the cation is finally coordinated to an amide O rather than to an Oe site. This is consistent with the solvation pattern seen in the other simulations viz the amide carbonyls are more exposed to the solvent and thus reside closer to the surface of the VM than the ester carbonyl groups. The displacement of the cation from the center of the VM (beginning at ~25 ps) is evidenced by the decay in the number of O, Os, and Oe groups in the second coordination sphere of the K^+. The coordination pattern seen after 45 ps is that which persisted until the final release at ~85 ps of simulation. In this state the K^+ was coordinated by six waters and one O ligand, with several VM ligands in the second coordination sphere. The long residence time of the Lac face water and the O ligand in the first coordination sphere of the cation before the final release arises because the VM places steric restrictions on the direction of further water attacks. Indeed final release occurred only when fluctuations in the local structures managed both to break one of

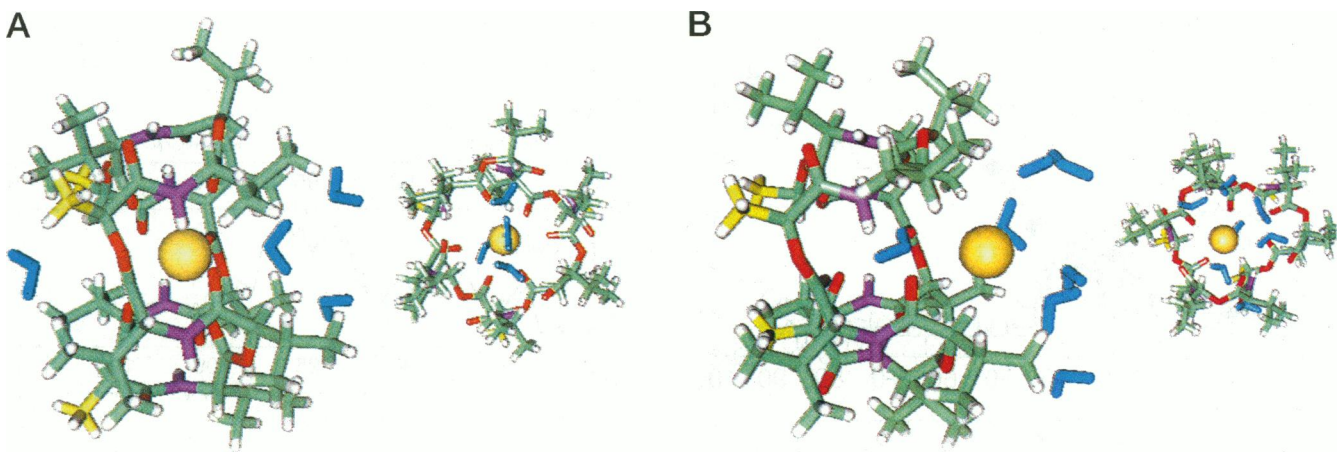

FIGURE 6 Snapshots along the K^+-VM decomplexation pathway in water. Color schemes and view orientations as in Fig. 2. The waters are shown in blue. Only water molecules within 6 Å of the K^+ are shown. (*a*) In the early stages water attack on the K^+ is evident through both Lac and HyV faces. The closest attack is through the HyV face. (*b*) Eventually the K^+ is drawn out through the HyV face and the Lac face water drawn into the center of the VM.

the Lac face water hydrogen bonds and disrupt the coordination of this water to the cation. Only then was the remaining VM · O ligand displaced by a water from the solvent. As the cation was drawn into the bulk water, VM sites were lost from the second coordination sphere within 10 ps leaving the cation solvated by seven waters in the first shell and ~20 in the second.

As already noted during the final release, the coordination of the K^+ to the Lac face water was lost. Fig. 8 shows the distances to the cation of this and one other water and to the last VM ligand as a function of time. The figure illustrates that the remaining carbonyl ligand [O(165)] is displaced from the first coordination sphere by the entry of Ow(742) from the bulk at ~83 ps. (The plot for Ow(742) also shows the lability of exchange between the first and outer coordination spheres of the K^+.) The Lac face water [Ow(637)] is displaced to the second coordination sphere 0.5 ps later and, subsequently, to the third coordination sphere. However, this water did leave the VM through the HyV face some 15 ps later and was seen to re-enter the first coordination sphere of the cation (t = 107 ps) when both were in the bulk.

The decomplexation event is of some significance as there is disagreement in the literature over which face is preferred for cation passage during (de-)complexation. Free energy perturbation studies in methanol (Åqvist et al., 1992) suggested the Lac face is the most prone to attack from solvent such as methanol, whereas potential of mean force calculations favored passage of K^+ through the HyV face (Marrone and Merz, 1995). In the aqueous case it appears that passage through the HyV face is favored. We are currently carrying out potential of mean force calculations to further characterize the mechanism. Nonetheless, our results do show some similarity with the methanol results of Marrone and Merz viz that solvent attack takes place through both faces and that metastable solvent adducts are formed along the decomplexation pathway. However, in the methanol case the most stable intermediate corresponded to cation coordination to an average of 3.3 VM carbonyls, whereas in water the adduct with only one VM ligand was the most long lived (an adduct with two to three VM ligands persisted for 15 ps, also).

Unfortunately there is little, if any, experimental data to resolve the discrepancy in the theoretical studies in methanol. The situation is little better for water. Although a monohydrate form of K^+-VM can be crystallized, the water is associated with the counterion rather than the potassium (Hamilton et al., 1981). However in the Na^+ analog the cation is displaced toward the Lac face to bind with the counterion while a water molecule resides in the centre of the VM cage (Steinrauf et al., 1982) suggesting that water attack occurs most readily through the HyV face.

Examination of structures along the reaction pathway suggest a simple explanation for the observed mechanism. As the cation moves through the HyV face, that orifice undergoes an expansion. To compensate the orifice at the opposite face, the Lac face contracts. An extreme form of the expansion/contraction behavior is seen in the TP solid-state conformer. There the orifice associated with the Lac face all but vanishes and the HyV face is completely open (Fig. 2 *c*). There are twice as many isopropyl groups in the neighborhood of the HyV orifice and steric hindrance strongly disfavors the alternative mechanism, which is contraction of the HyV orifice to allow opening of the Lac face.

The dihedral configurations of two minimized structures of Fig. 6 are given in Table 1. They are labeled as K^+-VM$(H_2O)_1$ and K^+-VM$(H_2O)_2$ designating the number of water molecules coordinating to the cation through the HyV face. The coordination of the first water is accompanied by only minor conformational changes in α_1 and α_2 from the K^+-VM structure. It is the close coordination of the second water through the HyV face that requires all the δ_2 dihedrals to change from $g+$ to $g-$. Subsequently the transition of the $\gamma_2(g+ \rightarrow t)$ allows

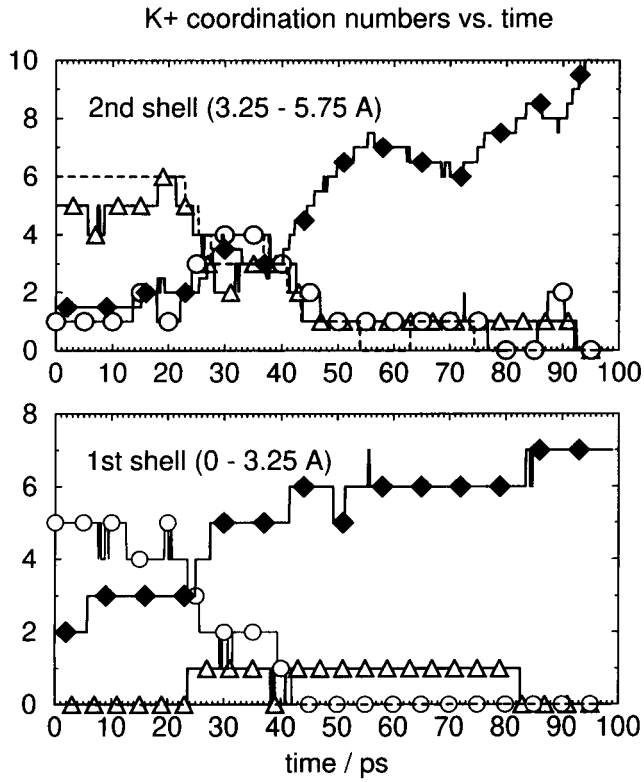

FIGURE 7 Potassium coordination as a function of time in the K^+-VM/water system in the first 100 ps of the production part of the simulation. First shell coordination numbers are evaluated out to 3.25 Å from the cation. The second shell was defined to be between 3.25 and 5.75 Å from the cation. To reduce statistical noise, coordination numbers are given as the average coordination number, rounded to the nearest integer, in a 1-ps window centered about each point in time. Note that in the second shell values for Ow (◆) have been divided by 2.0. Symbols for the VM sites are: Oe (○), O (△), and Os (--).

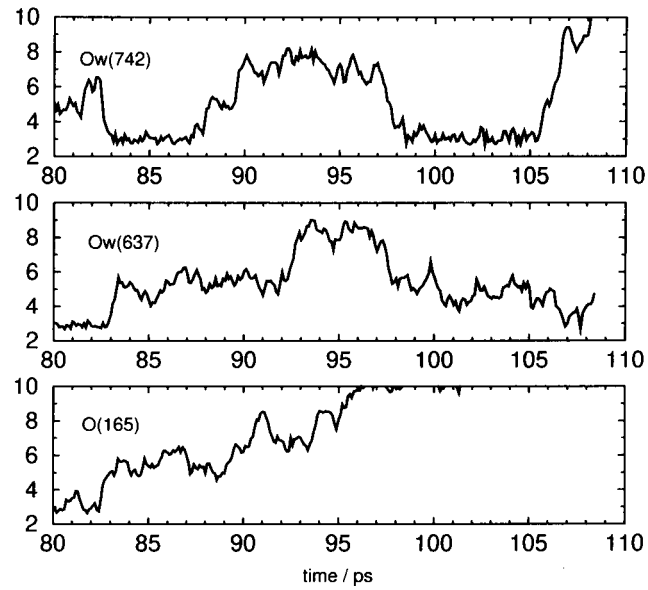

FIGURE 8 Selected K^+-O distances around the time of final release. O(165) is the last VM carbonyl to be coordinated to the cation; Ow(637) is the Lac face water and Ow(742) a water that coordinates to the cation from the bulk. The first coordination shell corresponds to distances around 3 Å the second coordination shell to those around 5 Å.

two, and then three, more waters to coordinate through the HyV face. Once this has taken place, exchange of the remaining VM ligand occurred when there were large fluctuations in one γ_1 (still $g-$) associated with the breaking of the Lac face waters first hydrogen bond. The remaining dihedral transitions to the VM(H_2O) structure (Table 1) involving $\alpha_2(t \rightarrow g+)$ were established on the same time scale as the final cation removal.

CONCLUSION

In agreement with experiment, the simulations show that the conformation of the K^+ complex in a nonpolar solvent is very similar to that in the solid state (Neupert-Laves and Dobler, 1975; Feigenson and Meers, 1980), but that the complex is unstable in water (Grell and Funck, 1975). In addition, the simulations confirm the conclusions from experimental data that uncomplexed VM in solution is different from any of the known solid-state structures; a dynamic equilibrium between a distribution of closely related conformers is suggested. The actual distribution is solvent dependent (Grell and Funck, 1975; Bystrov et al., 1977) and reflects the preferential solvation of either the hydrophobic or hydrophilic moities in the molecule. In nonpolar solvent, uncomplexed VM loses the distinctive Lac and HyV faces found in the solid state and the K^+-VM complex. In water the faces are retained and in resemblance to the TP solid-state structure VM adopts near trigonal symmetry. For our potential model, the time scale for the key dihedral transitions between the various complexed and uncomplexed conformers is ~100 ps.

In our simulations the decomplexation of K^+-VM in water is initiated by water molecule attack through both the faces of the complex. Rotation around the δ_2 dihedral angles in the three lactic acid residues provides a hinge effect, which allows the HyV orifice to open with further hydration and eventual removal of K^+. Opening of the HyV orifice is less sterically hindered than opening of the Lac face.

There is considerable interest in understanding the structure and reaction mechanisms of VM and K^+-VM at a membrane-water interface. The evidence suggests, however, that considerable care must be taken in drawing conclusions concerning such behavior from data obtained in homogeneous solvents. The lability of the solution structures and the sensitivity to hydrophobic and hydrophilic interactions makes accurate predictions very difficult.

We thank the Materials Consortium of the High Performance Computing Initiative of the EPSRC for an allocation of time on the Cray-T3D at Edinburgh and The Edinburgh Parallel Computing Centre for operational support. Daresbury Laboratory is thanked for use of the IBM SP2. TRF is supported by a grant to the Collaborative Computational Project (CCP5) from the former Science and Materials Computing Committee of the Engineering and Physical Sciences Research Council (EPSRC).

REFERENCES

Åqvist, J., O. Alvarez, and G. Eisenman. 1992. Ion-selective properties of a small ionophore in methanol studied by free-energy perturbation simulations. *J. Phys. Chem.* 96:10019–10025.

Berendsen, H. J. C., J. P. M. Postma, W. F. van Gunsteren, and J. Hermans. 1981. *In* Intermolecular Forces. B. Pullman, editor. Reidel. 331.

Bishop, M., and J. H. R. Clarke. 1991. System size dependence and time convergence in molecular-dynamics simulations of monolayer films. *J. Chem. Phys.* 95:540–543.

Bystrov, V. F., Y. D. Gavrilov, V. T. Ivanov, and Yu A. Ovchinnikov. 1977. Refinement of the solution conformation of valinomycin with the aid of coupling constants from the ^{13}C-nuclear-magnetic-resonance spectra. *Eur. J. Biochem.* 78:63–82.

Feigenson, G. W., and P. R. Meers. 1980. ^{1}H NMR study of valinomycin conformation in a phospholipid bilayer. *Nature.* 285:313–314.

Forester, T. R., and W. Smith. 1994. The DL_POLY User's Manual. Daresbury Laboratory. ref. no. DL/SCI/TM100T. Daresburg, Warrington WA4 4AD, UK.

Forester, T. R., W. Smith, and J. H. R. Clarke. 1994. A molecular-dynamics study of valinomycin and the potassium-valinomycin complex. *J. Phys. Chem.* 98:9422–9430.

Forester, T. R., W. Smith, and J. H. R. Clarke. 1995. Capture of potassium-ions by valinomycin: a molecular-dynamics simulation study. *J. Phys. Chem.* 99:14418–14423.

Grell, E., and T. Funck. 1975. Structure and dynamic properties of ion-selective antibiotics. *In* Membranes, Vol. 3. G. Eisemann, editor. Dekker, New York. 1–126.

Guba, W., and H. Kessler. 1994. A novel computational mimetic of biological-membranes in molecular-dynamics simulations. *J. Phys. Chem.* 98:23–27.

Hamilton, J. A., M. N. Sabesan, and L. K. Steinrauf. 1981. Crystal-structure of valinomycin potassium picrate-anion effects on valinomycin cation complexes. *J. Am. Chem. Soc.* 103:5880–5885.

Hoover, W. G. 1985. Canonical dynamics-equilibrium phase-space distributions. *Phys. Rev.* A31:1695–1697.

Ivanov, V. T., I. A. Laine, L. B. Senyavina, E. M. Popov, Yu A. Ovinnikov, and M. M. Shemyakin. 1969. The physiochemical basis of the functioning of biological membranes: the conformation of valinomycin and its K^+ complex in solution. *Biochem. Biophys. Res. Commun.* 34:803–811.

Jackson, M., and H. J. Mantsch. 1991. Valinomycin and its interaction with ions in organic solvents, detergents, and lipids studied by Fourier transform IR spectroscopy. *Biopolymers.* 31:1205–1212.

Karle, I. L. 1975. Conformation of valinomycin in a triclinic crystal form. *J. Am. Chem. Soc.* 97:4379–4386.

Karle, I. L., and J. L. Flippen-Anderson. 1988. A new conformation exhibiting near-threefold symmetry for uncomplexed valinomycin in crystals from dimethyl-sulfoxide. *J. Am. Chem. Soc.* 110:3253–3257.

Lau, K. F., H. E. Alper, T. S. Thacher, and T. R. Stouch. 1994. Effects of switching-functions on the behavior of liquid water in molecular-dynamics simulations. *J. Phys. Chem.* 98:8785–8792.

Marrone, T. J., and K. M. Merz. 1995. Molecular recognition of K^+ and Na^+ by valinomycin in methanol. *J. Am. Chem. Soc.* 117:779–791.

S. Melchionna, G. Ciccotti, and B. L. Holian. 1993. Hoover NPT dynamics for systems varying in shape and size. *Mol. Phys.* 78:533–544.

Neupert-Laves, K., and M. Dobler. 1975. The crystal structure of a K^+ complex of valinomycin. *Helv. Chim. Acta.* 58:432–442.

Perera, L., U. Essmann, and M. L. Berkowitz. 1995. Effect of the treatment of long-range forces on the dynamics of ions in aqueous-solutions. *J. Chem. Phys.* 102:450–456.

Roux, B., B. Prodhom, and M. Karplus. 1995. Ion-transport in the gramicidin channel—molecular-dynamics study of single and double occupancy. *Biophys. J.* 68:876–892.

Rudnick, J., and G. Gaspari. 1987. The shape of random walks. *Science.* 237:384–389.

Schreiber, H., and O. Steinhauser. 1992. Molecular-dynamics studies of solvated polypeptides: why the cutoff scheme does not work. *Chem. Phys.* 168:75–89.

Smith, W., and D. Fincham. 1993. The Ewald sum in truncated octahedral and rhombic dodecahedral boundary-conditions. *Mol. Simul.* 10:67–71.

Smith, W., and T. R. Forester. 1994a. Parallel macromolecular simulations and the replicated data strategy. 1. The computation of atomic forces. *Comp. Phys. Commun.* 79:52–62.

Smith, W., and T. R. Forester. 1994b. Parallel macromolecular simulations and the replicated data strategy. 2. The RD-SHAKE algorithm. *Comp. Phys. Commun.* 79:63–77.

Steinrauf, L. K., J. A. Hamilton, and M. N. Sabesan. 1982. Crystal-structure of valinomycin sodium picrate-anion effects on valinomycin cation complexes. *J. Am. Chem. Soc.* 104:4085–4091.

Weiner, S. J., P. A. Kollman, D. T. Nguyen, and D. A. Case. 1986. An all atom force-field for simulations of proteins and nucleic-acids. *J. Comp. Chem.* 7:230–252.